Electronic Supplementary Information

A nature-inspired solution for water management in flow fields for electrochemical devices

Panagiotis Trogadas[1†], Jason I. S. Cho[1†*], Lara Rasha[2], Xuekun Lu[2], Nikolay Kardjilov[3], Henning Markötter[3], Ingo Manke[3], Paul R. Shearing[2], Dan J.L. Brett[2], and Marc-Olivier Coppens[1*]

[1]EPSRC "Frontier Engineering" Centre for Nature Inspired Engineering, Department of Chemical Engineering, University College London, London, WC1E 7JE, UK
[2]Electrochemical Innovation Lab, Department of Chemical Engineering, University College London, London, WC1E 7JE, UK
[3]Helmholtz-Zentrum Berlin, Hahn-Meiitner-Platz 1, 14109, Berlin, Germany
†Both authors contributed equally
*Corresponding authors. Email: in.cho.13@alumni.ucl.ac.uk (J.I.S. Cho); m.coppens@ucl.ac.uk (M.-O. Coppens)

Section S1. Materials and methods

S1.1 MEA fabrication. An MEA with surface area of 10 cm^2 is synthesized in-house *via* hot pressing (12-ton thermal press, Carver, 4122CE) a Nafion® 212 membrane (50 μm thickness, DuPont, USA) in between two gas diffusion electrodes ELE0070 (0.4 g_{Pt} cm^{-2} loading, Johnson Matthey, UK). The MEA is pressed at 400 psi and 130 ^oC for 3 min. These experimental conditions are chosen for the fabrication of the MEAs to achieve optimal interfacial contact between the catalyst layer and the polymer membrane.[1] An ELE0070 gas diffusion electrode (Johnson Matthey, UK) is used in all experiments. Tygaflor gaskets (280 μm) are placed around each ELE to seal gases and prevent over-compression.

S1.2 PEMFC components. The PEMFC contains a commercial, single-serpentine flow-field (10 cm^2 surface area) at the anode with channel width, spacing, and depth of 1 mm, 1 mm, and 0.7 mm, respectively. At the cathode, four different flow-fields (10 cm^2 surface area) are used, namely commercial single- and double-serpentine flow-fields, LUCY, and a pristine lung-inspired flow-field with N = 4 generations, to evaluate the effectiveness of the water management strategy in the best performing lung-inspired flow-field, which has N = 4 generations for a 10 cm^2 surface area. A detailed description of its dimensions and manufacturing procedure are detailed elsewhere.[2] The single-serpentine flow-field used at the cathode has the same dimensions as its counterpart in the anode, while the double-serpentine and parallel flow-fields have channel width, spacing, and depth of 1.2, 1.2, and 0.8 mm, respectively.

A compact laser micromachining instrument (Oxford Lasers A Series, USA) is employed to engrave capillaries on a thin graphite plate (1.2 mm thickness). The laser engraved capillaries are 50 μm wide and 300 μm deep (Fig. 2(c)).

The laser process took a total of 25 min for 258 microchannels on a 10 cm^2 graphite plate.

This capillary array is then placed on to a graphite sheet (0.16 mm thick, 150 mm × 150 mm, RS series) with laser cut holes matching the fractal inlet holes of the lung-inspired flow-field. The fuel cell components were aligned with four alignment pins positioned at each corner of the rectangular arrangement. Compression alone is enough to seal these three components together.

S1.3 PEMFC operation. In the case of neutron measurements (Schematic S1), the PEMFC is placed vertically and operated without heating, while dry hydrogen and air are used as fuel and oxidant, with stoichiometric ratios of 1.2 and 3, respectively (Table S1). A DC electronic load regulates the current drawn from the fuel cell, while LabVIEW software (National Instruments) is used for data acquisition. These experimental conditions are purposely chosen to reproduce operating conditions limited by flooding, while preventing condensation within the fuel cell, which could block the through-plane view.[3] Galvanostatic measurements are conducted by gradually changing the current density every 10 min at 0.1 A cm^{-2} intervals until the potential falls below 0.2 V.

Table S 1. PEMFC operating conditions for neutron imaging and galvanostatic measurements.

Parameter	**Value**
Fuel cell temperature	Ambient
Anode RH	Dry
Cathode RH	Dry
Hydrogen stoichiometry	1.2
Air Stoichiometry	3
Active area	10 cm^2
Membrane	Nafion 212
Electrode	ELE0070
Anode and cathode outlet pressure	1 atm
Gas flow	Counter-current

In the case of PEMFC polarization measurements (Table S2) during which the cell is placed vertically, the relative humidity, inlet gas flow, and fuel cell temperature are regulated using an 850e fuel cell station (Scribner Associates, USA). The integrated potentiostat allows the measurement of membrane resistance. The stoichiometry at the anode and cathode are held constant at 1.2 and 3, respectively. The inlet gas relative humidity of the anode is the same as the cathode and the cell temperature is 70°C. The outlets of the anode and cathode are at atmospheric pressure.

Table S 2. PEMFC operating conditions for polarization measurements.

Parameter	**Value**
Fuel cell temperature	70°C
Anode RH	60, 80, 100
Cathode RH	60, 80, 100
Hydrogen stoichiometry	1.2
Air Stoichiometry	3
Active area	10 cm^2
Membrane	Nafion 212
Electrode	ELE0070
Anode and cathode outlet pressure	1 atm

Gas flow	Co-current

S1.4 Characterization of capillary array. The structure of the patterned thin graphite plate (1.2 mm thickness) with laser engraved capillaries is evaluated *via* X-ray tomography (Zeiss Xradia Versa 520, Zeiss, USA). The dimensions of the sample are 5 mm × 5 mm × 200 µm and it is imaged at 80 kV and 7 W beam power, an exposure time of 45 s per radiograph, and a 4x optical magnification with a pixel size of 2 µm. Avizo Fire software is used for the analysis of raw images and tomographic reconstruction of the acquired projection images is completed *via* the Gridrec algorithm after application of flat and dark field corrections.

To evaluate the hydrophilicity of the capillary array, Raman measurements are conducted for a pristine and a patterned graphite plate (1 cm × 1 cm dimensions) using a Renishaw InVia Raman microscope equipped with a laser of 785 nm.

Neutron radiography is conducted at the CONRAD neutron imaging facility at Helmholtz Zentrum Berlin with a flux of $2.7 \cdot 10^9$ neutrons $cm^{-2}s^{-1}$ and a maximum field-of-view of 3.5 × 3.5 cm^2. The PEMFC is positioned in through-plane orientation to the beam to visualize the formation of liquid water across the MEA. A 100 µm thick ^{6}LiF neutron scintillator converts the neutron flux into visible light, which is recorded by a CCD camera (Andor DW436N-BV, 2048 × 2048 pixels).[4] Images are taken with an exposure time of 5 s, which provides sufficient temporal resolution to track changes in liquid water distribution during a current hold.[3]

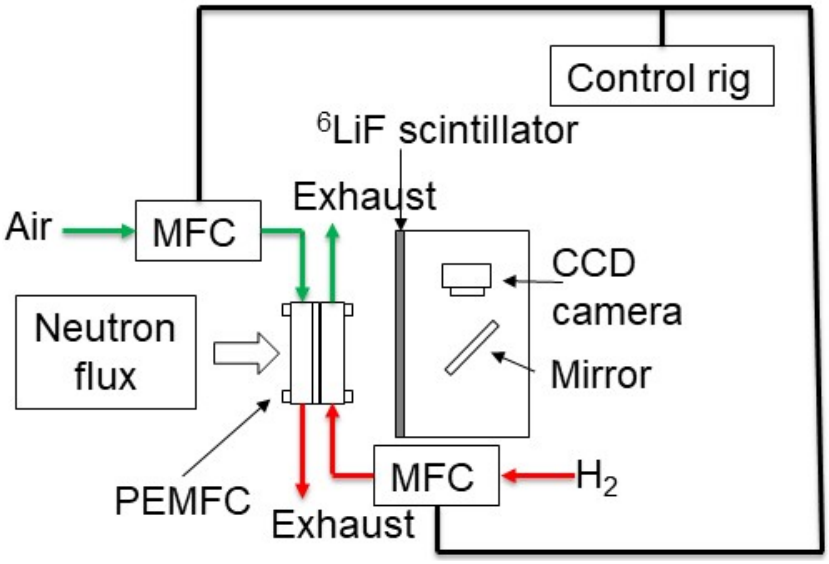

Schematic S 1. Simplified schematic for through-plane fuel cell imaging facing the ^{6}LiF scintillator. MFC stands for mass flow controller.

The obtained neutron images are normalized to a reference image of the dry PEMFC (Fig. S1) before operation to obtain only the attenuation corresponding

to the water content in the PEMFC. The thickness of water, t_{water}, is calculated from the relative neutron transmission (I/I_o) by inverting the Lambert-Beer law[3]:

$$t_{water} = -\frac{\ln\left(\frac{I}{I_o}\right)}{\mu_{water}} \qquad [S1]$$

where I is the intensity of the beam in operation, I_o is the intensity of the beam of the dry PEMFC, t_{water} is the thickness of water, and μ_{water} is the attenuation coefficient of water, which is equal to 3.5 cm^{-1}, based on the measurements at the CONRAD beamline.

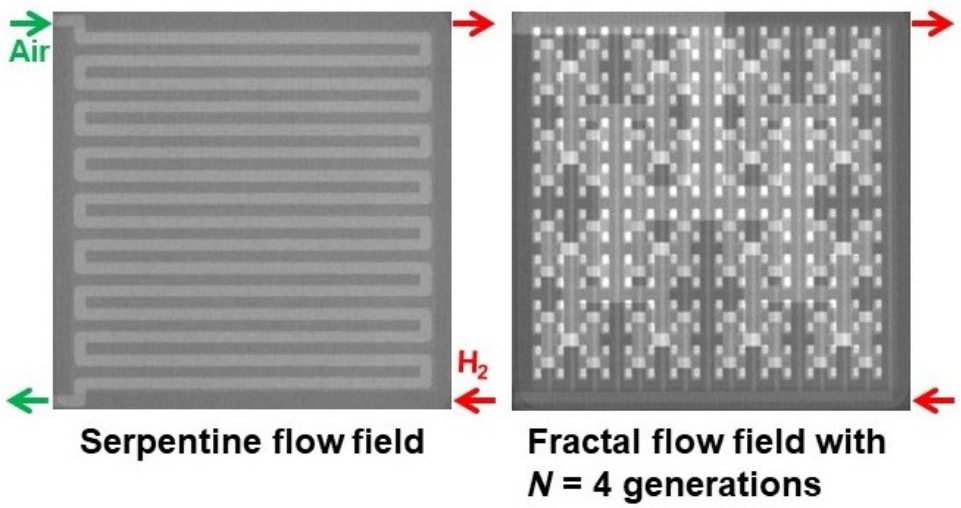

Figure S 1. *Radiograph of a dry cell with single serpentine flow-field, and lung-inspired flow-field (N = 4). Green and red arrows indicate the flow direction of air and hydrogen, respectively. In the case of a lung-inspired flow-field, air is directed perpendicular to the plane and the outlet is at the bottom left.*

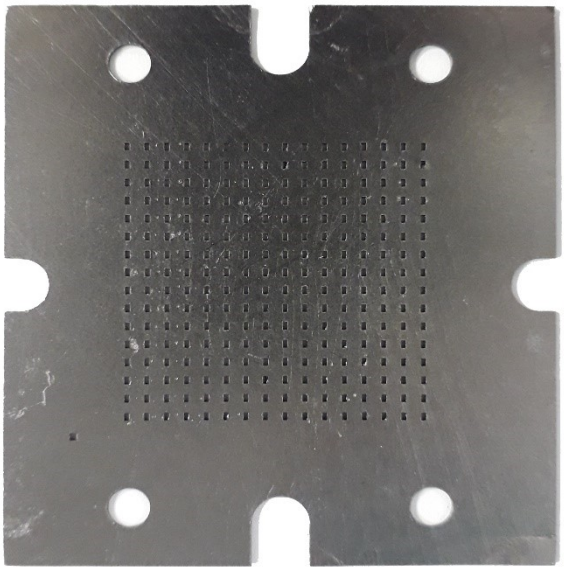

Figure S 2. *Engineered graphite gasket sheet sandwiched between the fractal flow-field and the graphitic capillary array.*

Section S2. Raman spectroscopy measurements

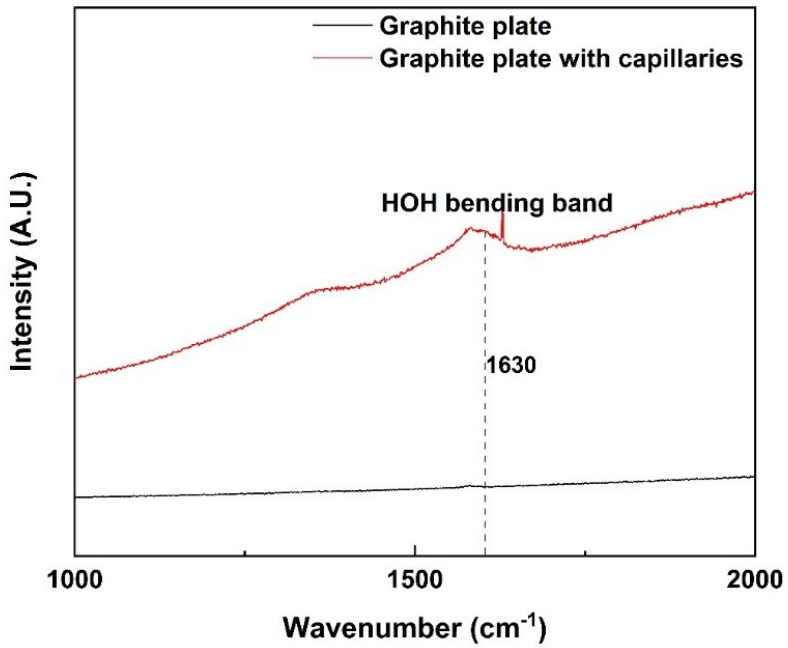

Figure S 3. *Raman spectra of pristine and patterned graphite plate with laser engraved capillaries (capillary array). The hydrophilic property of the latter is evident by the appearance of the H-O-H bending band.*

Section S3. Pressure drop measurements

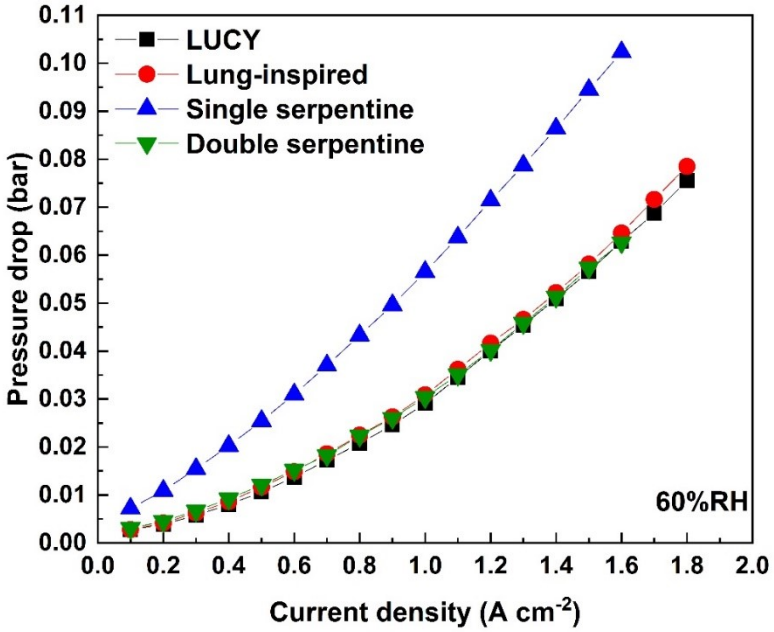

Figure S 4. Pressure drop of all different flow-field designs tested at 60% RH. Experimental conditions: H_2/Air stoichiometry = 1.2/3, 0.4 $mg_{Pt}cm^{-2}$ loading, 10 cm^2 flow-field area.

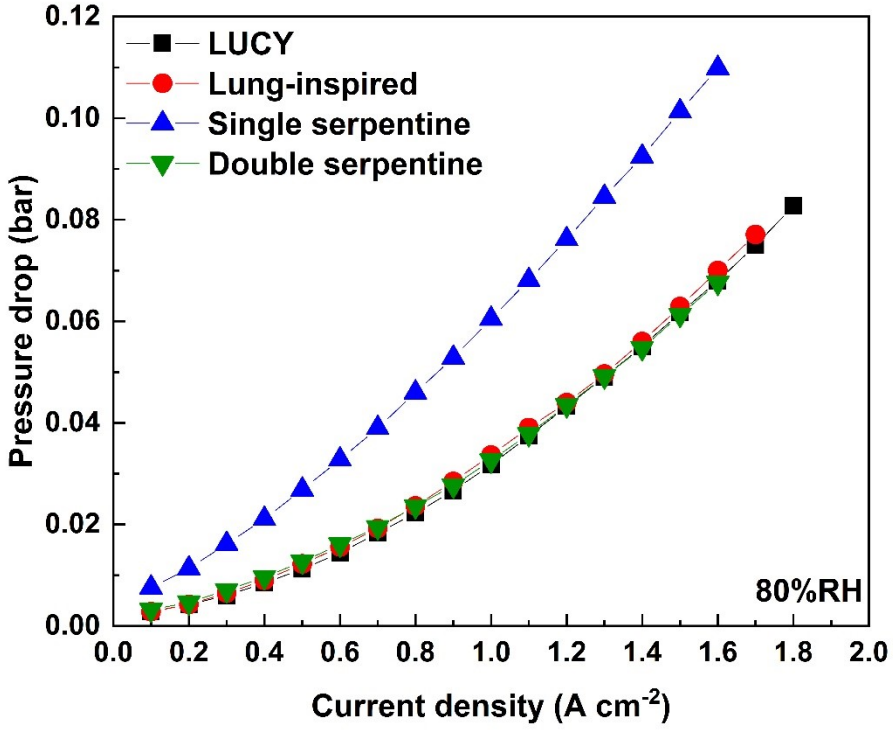

Figure S 5. Pressure drop of all different flow-field designs tested at 80% RH. Experimental conditions: H_2/Air stoichiometry = 1.2/3, 0.4 $mg_{Pt}cm^{-2}$ loading, 10 cm^2 flow-field area.

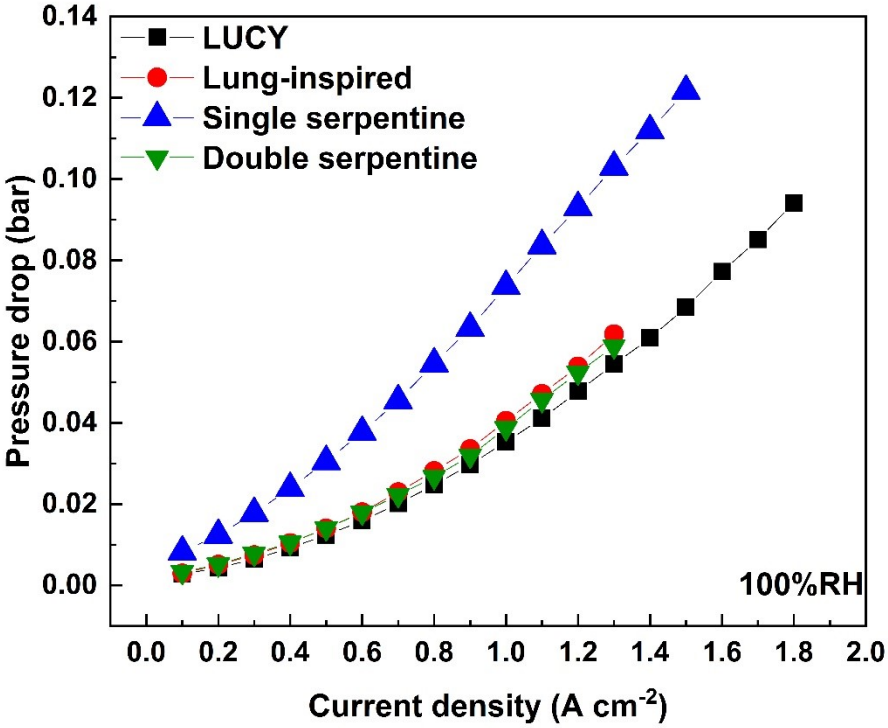

Figure S 6. Pressure drop of all different flow-field designs tested at 100% RH. Experimental conditions: H_2/Air stoichiometry = 1.2/3, 0.4 $mg_{Pt}cm^{-2}$ loading, 10 cm^2 flow-field area.

Section S4. Calculation of Bond and capillary numbers, and derivation of the simplified form of Young-Laplace equation

S4.1. Values used for the calculation of Bond and capillary numbers.

Table S 3. Data for the calculation of *Bo* and *Ca* numbers.

Physical symbol	Description	Value
γ	Surface tension of water	0.07 N m^{-1}
η	Dynamic viscosity of water	$8.9 \cdot 10^{-4}$ Pa s
ρ	Density of water	1000 kg m^{-3}
g	Gravitational acceleration	9.8 m s^{-2}
L	Characteristic length of the capillary	$L_{lizard} = 1.5 \cdot 10^{-4}\, m$ $L_{Patterned\ graphite} = 1.39 \cdot 10^{-3}\, m$
u	Water transport velocity within the capillary network	$u_{lizard} \sim 3 \cdot 10^{-3}\, m\, s^{-1}$ $u_{patterned\ graphite} \sim 2.3 \cdot 10^{-3} m\, s^{-1}$

S4.2. Derivation of simplified form of Young-Laplace equation

The pressure difference (*ΔP*) in such capillary can be described by the simplified Young-Laplace equation[5]

$$\Delta P = \gamma r^{-1} \qquad [S2]$$

where γ is the surface tension of water and r is the principal radius. The radius r can be calculated from

$$r = w\,(2\cos\,(\theta - \alpha))^{-1} \qquad \text{[S3]}$$

which is based on the width w of the capillary, the contact angle θ, and the tilt angle α of the capillary side walls.

Inserting eqn. [S3] into [S2] yields

$$\Delta P = 2\gamma\cos\,(\theta - \alpha)w^{-1} \qquad \text{[S4]}$$

Section S5. Membrane resistance measurements

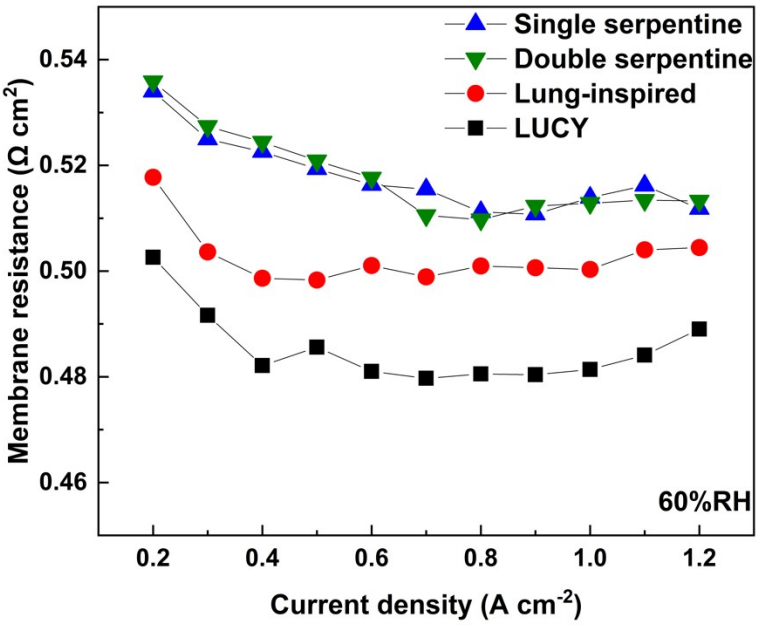

Figure S 7. Membrane resistance of all different flow-field designs tested at 60% RH. Experimental conditions: H_2/Air stoichiometry = 1.2/3, 0.4 $mg_{Pt}cm^{-2}$ loading, 10 cm^2 flow-field area.

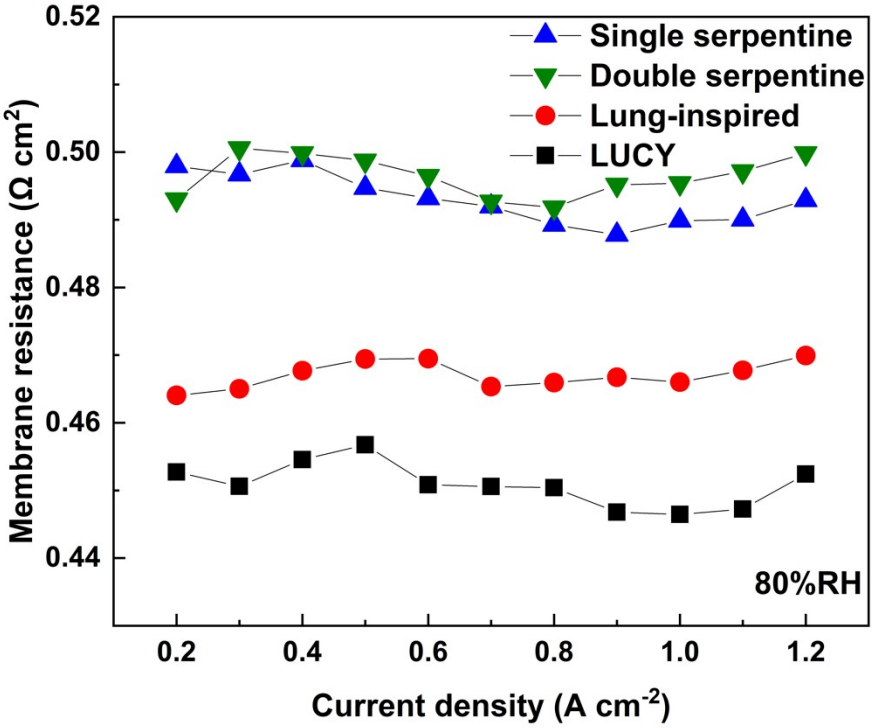

Figure S 8. Membrane resistance of all different flow-field designs tested at 80% RH. Experimental conditions: H_2/Air stoichiometry = 1.2/3, 0.4 $mg_{Pt}cm^{-2}$ loading, 10 cm^2 flow-field area.

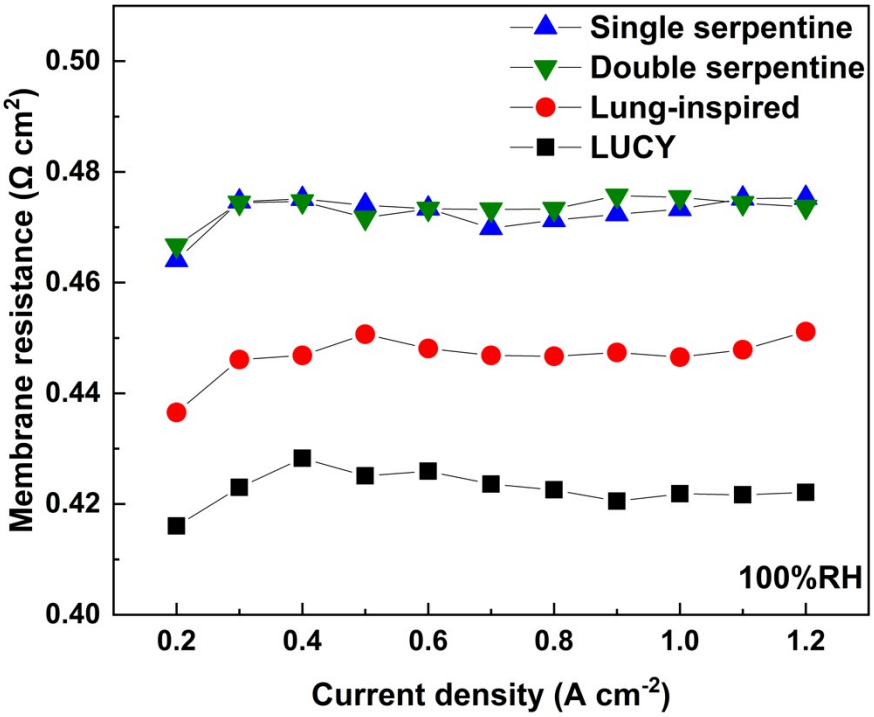

Figure S 9. Membrane resistance of all different flow-field designs tested at 100% RH. Experimental conditions: H_2/Air stoichiometry = 1.2/3, 0.4 $mg_{Pt}cm^{-2}$ loading, 10 cm^2 flow-field area.

References

1. P. Trogadas, J. I. S. Cho, N. Kapil, L. Rasha, A. Corredera, D. J. L. Brett and M.-O. Coppens, *Sustainable Energy & Fuels*, 2020, **4**, 5739-5746.
2. P. Trogadas, J. I. S. Cho, T. P. Neville, J. Marquis, B. Wu, D. J. L. Brett and M. O. Coppens, *Energy & Environmental Science*, 2018, **11**, 136-143.
3. J. I. S. Cho, T. P. Neville, P. Trogadas, Q. Meyer, Y. Wu, R. Ziesche, P. Boillat, M. Cochet, V. Manzi-Orezzoli, P. Shearing, D. J. L. Brett and M. O. Coppens, *Energy*, 2019, **170**, 14-21.
4. I. Manke, H. Markötter, T. Arlt, C. Tötzke, M. Klages, J. Haußmann, S. Enz, F. Wieder, J. Scholta, N. Kardjilov, A. Hilger and J. Banhart, *Physics Procedia*, 2015, **69**, 619-627.
5. P. Comanns, G. Buchberger, A. Buchsbaum, R. Baumgartner, A. Kogler, S. Bauer and W. Baumgartner, *Journal of The Royal Society Interface*, 2015, **12**, 20150415.